Journal of Petroleum Science and Technology 11(2): 30, 2021 2-12
DOI: 10.22078/jpst.2021.4414.1716

Journal of Petroleum Science and Technology

https:///jpst.ripi.ir/

Effect of Bifunctional Pt-Containing Al_2O_3-FeY Nanocatalysts on Ethylbenzene Transformation

Milad Rasouli[1], Nakisa Yaghobi[1]*, Masoud Rasouli[2]
1. Department of Petrochemical, Iran Polymer and Petrochemical Institute, (IPPI) Tehran, Iran
2. School of Chemical Engineering, College of Engineering, University of Tehran, Tehran, Iran

Abstract
Transformation of ethylbenzene can provide valuable isomers as a raw material for the petrochemical industry. This work explored the transformation of ethylbenzene (EB) over nanozeolite Y with the Si/Al ratio of 5. Fe ion exchange was carried out to modify the acidity of zeolites. The influence of platinum was investigated by the introduction of Pt-Al_2O_3. XRD, SEM, ICP, BET, FTIR, 27Al MAS NMR, NH3-TPD, and TG tests were applied for the characterization of physicochemical properties of prepared nanocatalysts. The slight decrease in the surface area of synthesized Fe-Y nanocatalysts indicated that the major part of iron was deposited in the catalyst structure. The addition of iron to the nanocatalyst structure resulted in increased strong acid sites and decreased weak acid sites. Reduction in weak acidity led to a lower coke formation rate and higher stability of FeY nanocatalysts. Results illustrated that the intensity of Lewis acidity decreased for all prepared nanocatalysts by increasing the iron content while the number of Bronsted acid sites increased. The addition of platinum-Al_2O_3 to the FeY nanocatalysts illustrated higher EB conversion and the same catalyst stability as FeY nanocatalysts. Nanozeolite Pt/Fe-Y composed of 0.1 wt.% platinum and 1.0 wt.% iron was obtained to be effective catalyst for EB transformation reaction. The prepared catalyst indicated adequate degree of EB conversion (61%) as well as 77.2% EB isomerization, 3.3% EB disproportionation, 1.4% EB dealkylation, 3.1% EB cracking, 14.8% EB hydrogenation and 0.2% EB transalkylation.

Keywords: Nanozeolite Y, Fe Ion Exchange, EB Conversion, Pt Impregnation.

Introduction
Para-xylene (PX) is considered an important intermediate in producing fibers, films, and resins. This isomer is mainly produced through C8 aromatics resulting from naphtha reforming and steam cracking. This isomer has more than an 80% demand rate while only 25% is present in the xylene equilibrium mixture [1-5]. Therefore, the conversion of other isomers, including ethylbenzene, into this valuable isomer is of great importance in the petrochemical industry. PX can be separated through adsorption or crystallization, in which the residual mixture enters the xylene isomerization unit to gain more PX [6-8]. The C8 aromatics isomerization processes are different due to the way of EB conversion. EB can be converted to xylenes by isomerization or to benzene and ethylene by dealkylation. EB isomerization is a complicated reaction of bifunctional catalysis that depends on catalyst acidity adjustment [9-12].
EB isomerization over bifunctional catalysts can occur through the formation of traces of ethylcyclohexanes (ECHE) through hydrogenation of EB, acidic isomerization of reactive ECHE to dimethylcyclohexanes (DMCHE), and finally, dehydrogenation of DMCHE to xylenes [13].
Zeolites are widely used in chemical processes such as isomerization because of their special physicochemical properties such as large surface area, pore volume, adjustable acidity, and high catalytic stability [14-17]. Large pore size zeolites result in the conversion of EB to xylene, whereas medium-pore zeolites lead to disproportionation and dealkylation of this isomer. Various zeolite catalysts with different acidic structures and properties have been studied in ethylbenzene isomerization reactions in the literature [18-21], except the Y nanozeolite. Y zeolite indicates a faujasite (FAU) molecular sieve with a three-dimensional tetrahedral framework and a pore diameter of 7.4 Å [22].
Moreau and coworkers studied the Ethylbenzene Isomerization on Bifunctional Platinum Alumina–Mordenite Catalysts. The transformation of ethylbenzene was carried out on intimate mixtures of 0.5 wt% Pt/Al_2O_3 (75 wt%) with a platinum dispersion of 100% and of HMOR zeolites (25 wt%) with Si/Al ratios between 6.6 and 180. Best result for EB isomerization obtained

**Corresponding author:* Nakisa Yaghobi, Department of Petrochemical, Iran Polymer and Petrochemical Institute, Tehran, Iran, Tehran, Iran
E-mail addresses: n.yaghobi@ippi.ac.ir
Received 2021-02-14, Received in revised form 2021-08-24, Accepted 2021-09-06, Available online 2021-12-08

to be 67.9% over PtA-HMOR catalyst with Si/Al = 120 [23]. Bhavani et al. [24] investigated the Hydroisomerization of ethylbenzene over bimetallic bifunctional zeolite catalysts. They revealed that Ni addition up to 0.3 wt.% over 0.1 wt.% Pt/H-β and 0.1 wt.% over 0.1 wt.% Pt/H-MOR increases the ethylbenzene conversion, isomerization selectivity and sustainability of the catalysts.

Tsai et al. [25] studied the effects of modification of H-ZSM-5 on its catalytic performance in the conversion of ethylbenzene (EB). They reported that the methods of silica chemical vapor deposition and 5,6-benzoquinoline adsorption can inactivate the external surface of ZSM-5, thus suppressing disproportionation and transalkylation side reactions with which isomerization selectivity and xylene yield increase at the expense of EB conversion and p-xylene yield.

In this paper, for the first time, the bifunctional nanocatalysts constituted of Pt/Al_2O_3 (PtA) and Fe ion-exchanged Y zeolite with different amounts of iron were used to investigate the ethylbenzene isomerization reactions. The main emphasis was on reducing unwanted side effects, including EB disproportionation and transalkylation by optimizing nanocatalyst acidity through iron loading and the effect of Pt particles on the improvement of catalyst efficiency in the EB isomerization process.

Materials and Methods

Catalyst Synthesis

Nanozeolite Na-Y (Si/Al = 5) was prepared through hydrothermal synthesis [26]. The 500 ml of NH4NO3 solution (1 mol L^{-1}) was prepared and used for ion exchange 20 g nanozeolite Na-Y support at the temperature of 85 ºC for 10 h. The H-type of catalyst was achieved by calcination of NH_4-Y powders through calcination at 550 ºC for 12 h in the presence of air (5 ml min^{-1}).

Fe (III) chloride hexahydrate ($FeCl_3.6H_2O$) was used as a Fe precursor to prepare Fe-Y nanocatalysts. In this regard, a specified amount of nanozeolite Y powder was added to the iron solution (100 ml solution/ g zeolite) to obtain Fe-Y nanocatalysts with 0.2, 0.5, and 1 wt.% of iron which are abbreviated as 0.2FY, 0.5FY, and 1.0FY respectively. The ion exchange process was conducted at 80-90 °C for 24 h while stirring at 500 rpm. After the filtration and washing with distilled water, the prepared nanocatalysts were dried at 100 °C for 12 h.

For the preparation of PtA sample, γ-Al_2O_3 support was ion-exchanged with hexachloroplatinic acid solution (1 mol.L^{-1}) followed by calcination at 550 °C in the artificial air for 4 h (heating rate of 3°/min). The final PtA-FeY nanocatalysts were provided by physically mixing two components (PtA and FeY) for 6 h.

Catalyst Characterization

ICP-AES analysis was used to investigate the elemental analysis of nanocatalysts. The textural characterization of the prepared nanocatalysts such as surface area (SBET) and pore volume (Vtotal) was performed at P/P0=0.99 and 77 K through nitrogen adsorption on a gas adsorption analyzer (Micrometrics, ASAP 2010).

X-ray diffraction (XRD) was performed on a D8 Advanced Bruker AXS diffractometer with CuKα radiation at 40 kV and 40 mA in the range of 2θ = 5º-50º to investigate the structure and crystallinity of nanocatalysts. ^{27}Al MAS NMR was recorded on a Bruker Avance III (11.7 T) spectrometer operated with 130 MHz frequency and a spinning rate of 14 kHz. Perkin Elmer system 2000 spectrometer was applied to measure FT-IR spectra. Before the test, 10 mg of zeolite powder was pressed into a 16 mm diameter self-supporting wafer. The pyridine adsorption test was applied for estimating the Brönsted and Lewis acidity in the synthesized nanocatalysts.

The morphology of prepared nanocatalysts was investigated through Scanning Electron Microscopy (SEM) images recorded on Leica Cambridge S360.

NH_3-TPD was measured on a chemisorption analyzer (Micrometrics, ChemiSorb 2720). Before the test, 100 mg of the powdered sample was pretreated in the presence of helium (30 ml/min) at 500 °C for 1 hour. The samples were then saturated in the presence of ammonia (30 ml/min) at 25 °C for 20 min.

A thermogravimetric (TG) experiment was used to determine the amount of coke formation in the nanocatalysts after the reaction. The test was recorded on a Pyris Diamond instrument with 100 ml/min airflow at 750 ºC. 50 mg of each powder was pretreated in the N2 flow of 100 ml/min at 150 ºC until no weight loss was observed. Finally, desorption of ammonia was conducted at 100-600 °C.

Catalytic Performance

To investigate the EB transformation reactions, the prepared nanocatalysts were tested in a single-pass stainless steel fixed-bed reactor (i.d., 1 cm; length, 60 cm). The schematic of the experimental setup is displayed in Figure 1.

About 1 g of 100-500 µm mesh-sized nanocatalysts was used for the activity test. EB was injected into the plug flow reactor through a dosing system (ELDEX, 0.002 - 80 ml/min), and the feed gas mixture was delivered by a calibrated mass flow meter (BROOKS-SLA5800). The reaction was performed at the temperature of 400 °C, the pressure of 8 bar, and WHSV space velocity of 2.5 g EB g^{-1} h^{-1} of nanocatalyst. The composition of final products was analyzed at the time on stream (TOS) of 1h using an online three-column gas chromatograph equipped with a 25 m FFAP capillary column.

Results and Discussion

Characterization of Fe-Y nanocatalyst

Structural Characteristics

XRD patterns for the parent and Fe ion-exchanged Y nanozeolites are indicated in Figure 2, and the patterns revealed that all prepared samples indicated FAU type structure at 2θ values of 6, 10, 12, 15, 18 and 21 [27]. The effect of Fe incorporation on the nanocatalyst structure was studied. It was anticipated that Fe oxides would obviously be detected. However, it should be considered that no peaks ascribed to iron oxides were determined for FY nanocatalysts (0.2FY, 0.5FY, and 1.0FY). Proper distribution of iron in the pores and nanocatalysts surfaces and differences in the signal intensity of the Y zeolite and iron oxide are the main reasons for the impedance in detecting oxide peaks [26, 28-30].

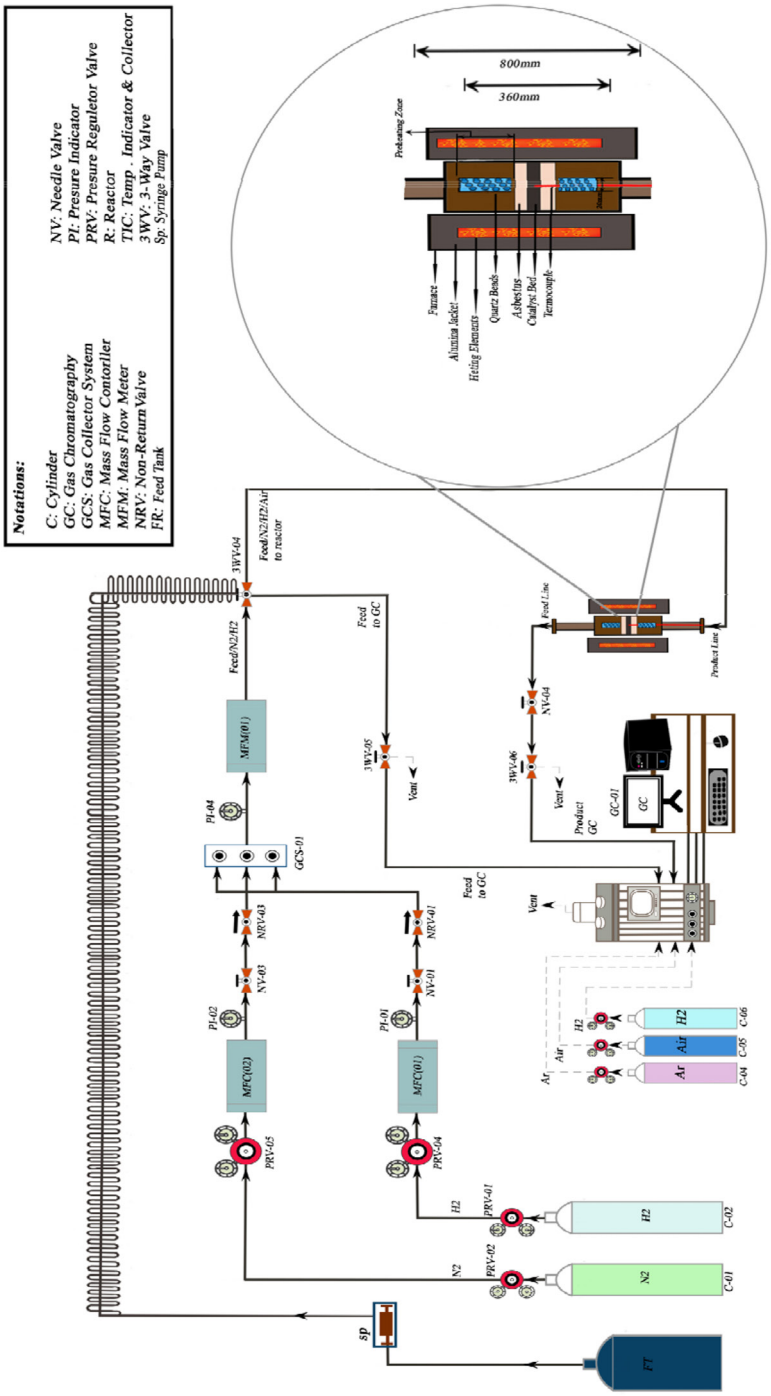

Fig. 1 Schematic of experimental Setup.

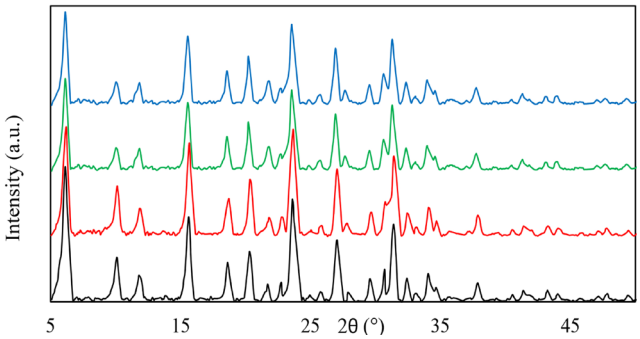

Fig. 2 XRD spectra of the (A) parent HY, (B) 0.2FY, (C) 0.5FY, (D) 1.0FY.

According to the peaks shown in Figure 2, all the samples indicated a similar crystalline structure to zeolite Y. The slight intensity reduction of some peaks could be attributed to a higher iron oxide absorption coefficient for X-ray radiation [31, 32]. As shown in Figure 1, there are no shifts in the peak position to the high 2θ values, which reveals no defects ascribed to the dealumination of catalysts through Fe ion exchange [33].

The slight decrease in crystallite size of modified nanocatalysts can be interpreted by the fact that the presence of iron particles has caused some influence on the crystallinity of Y zeolite [34]. These findings are in agreement with the XRD results.

SEM images of the parent and ion-exchanged Fe-Y nanocatalysts are presented in Figure 3. The morphology of synthesized Y powders demonstrated hexagonal crystallites with an average crystal size of 30 nm. The distribution of the crystals in the parent and modified Y nanozeolites was uniform, and no agglomeration was observed. It can be seen that Fe addition did not influence the catalyst morphology. The invisibility of the metal particles on the catalyst surface indicates that most of the iron particles are embedded in the zeolite cavities and channels.

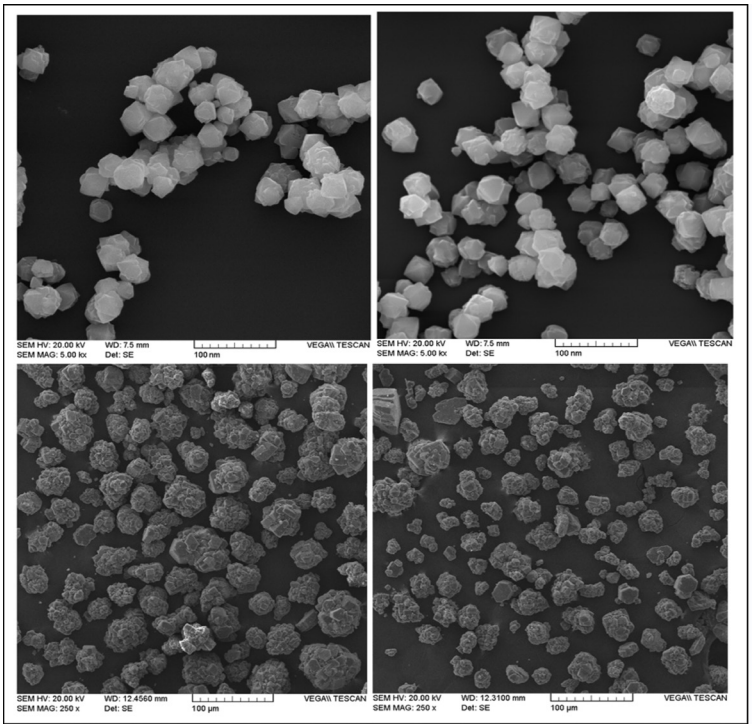

Fig. 3 SEM micrograph of different sample; (A) HY, (B) 0.2FY, (C) 0.5FY, (D) 1.0FY.

The elemental analysis and textural properties of nanocatalysts are presented in Table 1. The introduction of Fe ions into zeolite Y slightly reduced the surface area from 786.23 m^2/g for the nanozeolite H-Y to 782.65, 774.58 and 763.89 m^2/g for 0.2FY, 0.5 FY and 1.0 FY, respectively. The very slight decrease in the surface area of synthesized Fe-containing nanocatalysts indicated that the major part of iron is in the catalyst structure and a small amount of it is on the surface of the samples. This is because the entry of iron species into the micropores of the catalyst will occupy the empty space and consequently decrease the surface area. Kondru et al. [35] reported the BET surface area of zeolite HY reduced from 433 to 423 m^2/g after adding Fe ions. The results align with the findings of Aravindhan et al [36], which noticed that the introduction of large amounts of active metal into the nanozeolite Y cavities reduces its surface area. The total volume of synthesized nanocatalysts is also shown in Table 1.

The slight decrease in the pore volume of the Fe-modified Y nanocatalysts in comparison with the parent nanozeolite HY was in line with the results of the surface area analysis. The main reason for this phenomenon can be attributed to the smaller size of the iron ions located into the nanozeolite Y, which prevents micropore damage or pore blockage. According to all characterization data, it can be obviously inferred that the attachment of iron to Y zeolite was successfully achieved by the ion-exchange method.

Table 1 Elemental composition and textural characterization of different nanocatalysts samples.

Sample	Crystallinity (%)	Si/Al	S_{BET} (m^2g^{-1})	V_{total} (cm^3g^{-1})
HY	99.88	5	786.23	0.264
0.2Fe-Y	99.53	4.91	782.65	0.255
0.5Fe-Y	98.45	4.78	774.58	0.248
1.0Fe-Y	98.21	4.72	763.89	0.237

^{27}Al MAS NMR Spectroscopy

In Figure 4, the 27Al MAS NMR spectra for prepared Y nanocatalysts are shown. In the synthesized nanozeolites, aluminum is located not only in the tetrahedral framework (AlIV) (58 ppm) but also in the octahedral position (0 ppm) as extra framework aluminum (AlVI) [37]. Al was found to be mainly tetrahedrally coordinated in all samples. It can be seen that the intensity of the line at 59 ppm slightly decreases with an increase in the amount of Iron content, while no significant changes were observed at 0 ppm (extra-framework Al). It should be noted that extra-framework Al species have not replaced the loss of framework aluminum in Fe-containing nanocatalysts. This theme shows that part of the Al aluminum framework was transformed into NMR invisible Al species.

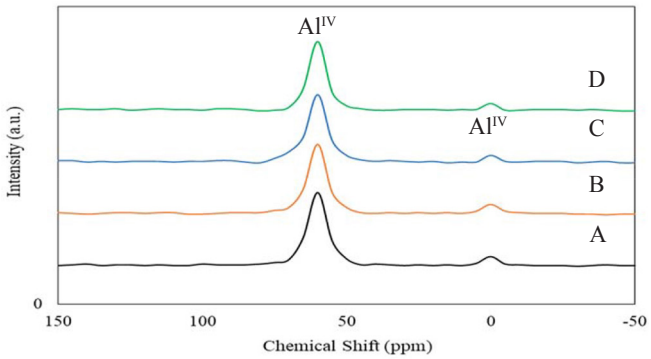

Fig. 4 27Al MAS NMR spectra of the (A) HY, (B) 0.2FY, (C) 0.5FY, (D) 1.0FY.

FT-IR Spectroscopy

According to the FT-IR spectrum of the parent and FeY nanocatalysts (Figure 5), no changes were happened to the zeolite structure through ion exchange and impregnation processes. The double ring-opening vibration at 565 cm^{-1} in the FT-IR spectrum of nanozeolite Y is characteristic of faujasite zeolites [38]. The T-O bending vibrations of internal tetrahedral in H-Y nanocatalyst can be distinguished by absorption bands around 500, 465 and 450 cm^{-1} [39]. The T-O bands attributed to symmetrical and asymmetrical stretching appeared at 1020 and 792 cm^{-1} [40]. The bands related to OH groups of water (3189 cm^{-1}) and C-O-H bend of water (1401 cm^{-1}) disappeared completely after calcination of Fe-modified nanozeolites at 500 °C. The absorption band that appeared at 1640 cm^{-1} could be attributed to the OH bending vibration [40, 41]. All absorption bands observed for the as-synthesized nanozeolite Y agree well with the IR spectra of zeolite Y reported in the literature [26, 42].

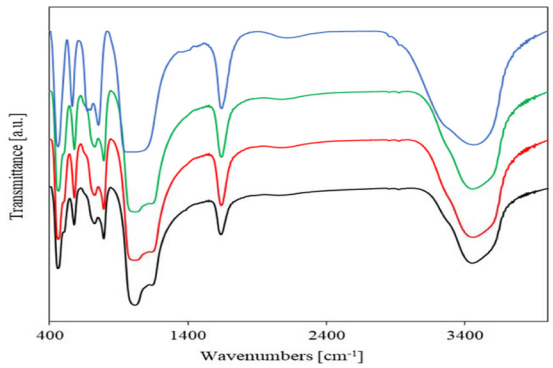

Fig. 5 FTIR spectra of different samples; (A) HY, (B) 0.2FY, (C) 0.5FY, (D) 1.0FY.

The IR intensity peak at 3466 cm^{-1} characterizing the Brönsted acidity was increased for all Fe-Y nanocatalysts compared to parent HY nanozeolite, which is similar to literature [39, 41] and corresponds to NH3-TPD results.

It can be seen overall that the main zeolite bands are still present in the parent H-Y nanozeolite after modification with iron which confirmed that ion exchange of the H-Y nanozeolite with Fe ions did not affect the zeolite structure.

Results obtained from the pyridine adsorption are given in Figure 6. The adsorption data are illustrated in the range of 1400-1600 cm^{-1}, where the vibration peaks corresponded to Brönsted and Lewis acid sites at 1543 cm^{-1} and 1450 cm^{-1}, respectively.

As illustrated, nanozeolite HY contains Brönsted and Lewis acid sites. Peaks around 1491 cm-1 are related to both Brönsted and Lewis acid sites. In Fe-Y nanocatalysts, the amount of Brönsted sites (1543 cm−1) is significantly increased, whereas the opposite for Lewis acidic sites that happened (1450 cm^{-1}) is observed. The results also show that the intensity of Lewis acidity has decreased for all prepared nanocatalysts, and an increase in the iron content increased the number of Bronsted acid sites.

Considering out-of-frame iron species, which contain only a small amount of acidic sites, the results show that the iron species are embedded in the catalysts framework structure.

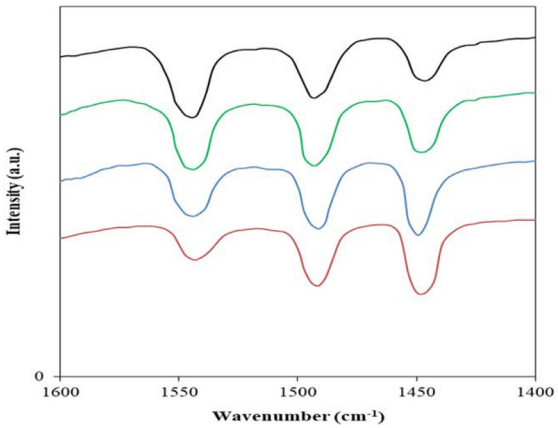

Fig. 6 IR spectra of pyridine adsorption for; (A) HY, (B) 0.2FY, (C) 0.5FY, (D) 1.0FY.

Acidity

Figure 7 indicates the NH3-TPD measurements of the parent HY and Fe ion-exchanged catalysts. The ammonia desorption band for HY-Nanozeolite in the region of 200-600 °C can be deconvoluted into 150-230, 270-410, and 450 °C centered peaks which are assigned to weak, medium, and strong acidity, respectively [43].

The amount and strength of acid sites of the nanocatalysts are given in Table 2.

The relative intensities of the abovementioned sub-peaks changed significantly through Fe loading. The data indicate that in iron-exchanged nanozeolites, the ammonia desorption is reduced at low temperatures due to the degradation of weak and medium acidic sites. On the other hand, an increase of iron content in the nanocatalyst structure increased the Brönsted acid sites due to the formation of new Brönsted sites derived from extra-framework aluminum species.

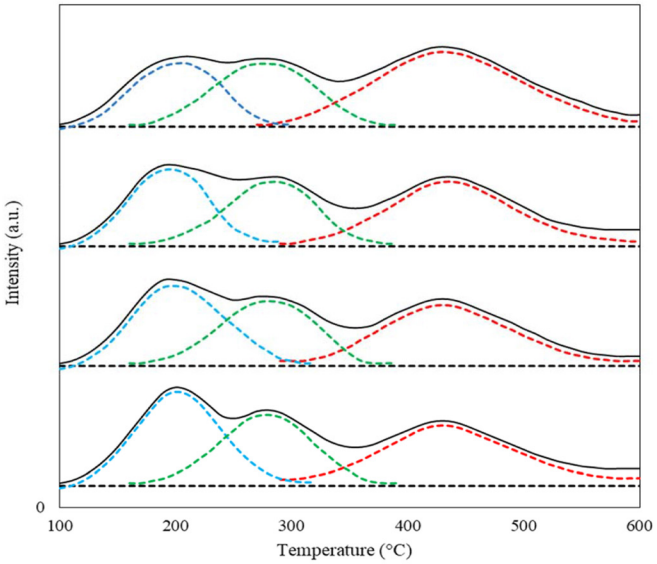

Fig. 7 NH3-TPD curves of different sample; (A) HY, (B) 0.2FY, (C) 0.5FY, (D) 1.0FY.

Table 2 Acidity sites of different nanocatalysts samples.

Catalyst	Acidity sites (mmol NH_3 g^{-1})			Total
	Weak	Medium	Strong	
HY	0.35	0.51	0.42	1.28
0.2FY	0.29	0.47	0.58	1.34
0.5FY	0.24	0.49	0.65	1.38
1.0FY	0.19	0.39	0.81	1.39

The quantification results of NH3-TPD (Table 2) demonstrated that the number of acidic sites on Fe-containing Y nanocatalysts changed through Fe-exchanging. The highest amounts of medium acid sites (0.51) and strong (0.75) acid sites were observed in the nanocatalysts 0.5FY and 1.0FY, respectively. By increasing the amount of iron in the nanocatalyst structure, ferrocene molecules react more with weak acid sites and reduce the number of such sites while forming strong acid sites.
Brönsted sites as main places for catalytic reactions [44] are usually present in the catalyst pore structure. On the other hand, Lewis acid sites play a key role in the coke formation in catalysts [45,46]. While enhancing in Brönsted acid sites leads to adverse side reactions, a decrease in weak acidity is necessary to reduce coke deposition and increase catalyst stability.

Catalyst Performance

The EB isomerization reaction takes place on a bifunctional catalyst substrate, whereas the EB dealkylation and disproportionation reactions largely depend on the acidic part of the catalyst [47]. Therefore, the balance between the acid and metal sites of the prepared nanocatalysts is of great importance in the EB isomerization process. Xylene isomerization catalysts comprising MFI molecular sieves always show some side reactions. Some methyl transfer (xylene disproportionation that forms TMB and methyl transfer to EB forming methylethylbenzenes (MEB)) happens, presumably at channel intersections as mentioned above. Also, for EB dealkylation catalysts, hydrogenation of the ethylene intermediate is not 100%. Thus, some ethyl transfer to xylenes occurs, which leads to xylene loss via the formation of dimethylethylbenzenes (DMEB) [48].
The EB transformation mechanism (Figure 8) is started by ring protonation (A→B) over a Bronsted acid site (S1). However, in this case, before the first ring cleaves, a second aromatic comes, and a bond begins to form.
The EB transformation mechanism (Figure 8) is started by ring protonation (A→B) over a Bronsted acid site (S1). However, in this case, before the first ring cleaves, a second aromatic comes, and a bond begins to form.
Several things are happening at the same time with intermediate N. EB transformation mechanism can be explained as; Protonation of the ring of the first EB is occurring; the bond to the ethyl side chain to the first EB begins to weaken; before the ethyl side chain leaves, a bond to the second EB begins to form; the bond between the ethyl side chain of the first EB breaks, and benzene (E) is liberated as the first byproduct; This leaves a ring protonated positively-charged diethylbenzene carbonium ion (F) as the zeolite framework charge compensating ion; This intermediate decomposes (F → S1), which regenerates the Bronsted acid site (S1), and diethylbenzene (G) releases into the gas phase as the second byproduct.
The conversion of ethylbenzene was performed using synthesized nanocatalysts containing 20 wt.% of FeY and 80 wt.% of Pt/Al_2O_3 (0.5PtA). The influence of catalyst acidity changes on the performance of Fe-Y and bifunctional PtA/FeY nanocatalysts is shown in Figure 9. Based on the results, the decrease of Lewis acidity during the ion exchange process with iron and enhancement in the Brönsted acidity in FeY nanocatalysts, inferred from FTIR and NH_3-TPD analysis, significantly increased the conversion of EB (Figure 9 A).

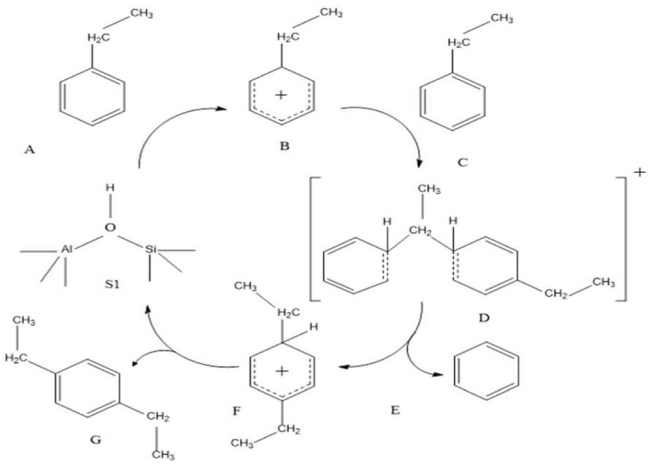

Fig. 8 Mechanism of EB transformation over PtA-FY catalysts.

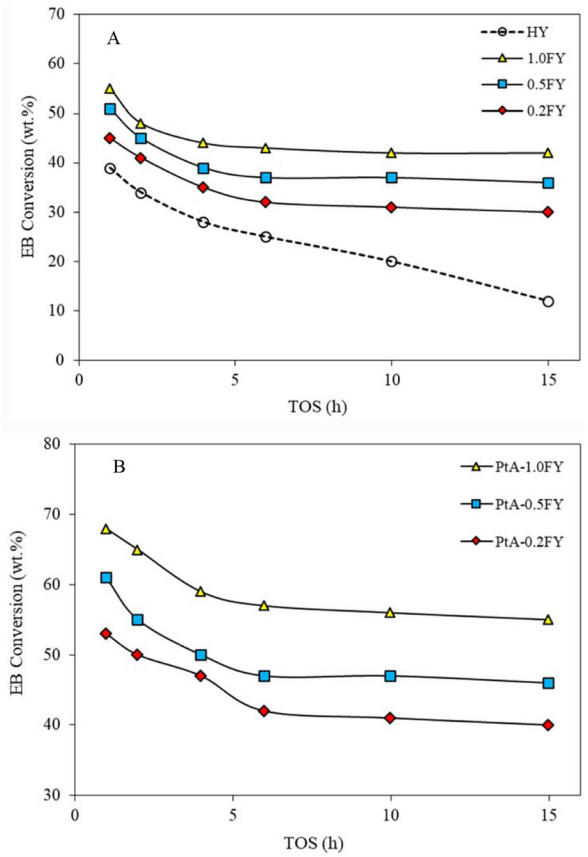

Fig. 9 EB conversion over; (A), FY catalysts and (B), PtA-FY catalysts

Moreover, incorporation of PtA to FeY nanozeolites demonstrated higher EB conversion than the FeY acid nanocatalysts (Figure 9 B).

The increase in the percentage of the Fe ion on the nanozeolite Y causes an increase in the selectivity to disproportionation as well as dealkylation and cracking. The main reason for this increase can be ascribed to unwanted reactions such as EB dealkylation and disproportionation at acidic sites of nanocatalyst, as well as the increase in Brönsted acid sites, which is the main driving factor of the isomerization reaction [49]. Platinum has been recognized as an effective agent in the EB to xylene conversion process, and the zeolites containing this noble metal have been extensively studied in EB transformation reactions [50, 51]. The distribution of the reaction products using prepared nanocatalysts was compared at EB conversion of 35% and is given in Table 3. The introduction of PtA into Fe-Y nanocatalysts led to an increase in the selectivity to isomerization and hydrogenation while diminishment occurred in the selectivities to other side reactions. One of the main reasons for the decrease in the rate of dealkylation and disproportionation reactions can be due to ethylene hydrogenation. The lower rate of disproportionation reaction can also be attributed to the lower concentration of benzylic carbocations. It has been reported by Gnep et al. [52] that if hydrogen is activated with metal, it will react with benzylic carbocations, and subsequently, it reduces the selectivity of disproportionation. It could be concluded by Moreau et al. [53] that disproportionation, dealkylation, and transalkylation of EB can take place on the acid catalyst, the hydrogenation of EB over metal catalysis and, isomerization and cracking of EB can take place over bifunctional catalysis. According to the data given in Table 3, it can be stated that the increase in Fe loading enhanced the amount of hydrogenation, which can be concluded by the fact that iron particles may act as hydrogenation agents. With the constant amounts of PtA, EB isomerization has been increased by the increase in Fe loading (from 58.5% in PtA/0.2FeY to 77.2% in PtA/1.0FeY) which is due to the synergistic effect of platinum and iron.

PtA-FeY nanocatalysts are found to be efficient catalysts for EB isomerization reactions. The EB isomerization process contains a series of consecutive reactions; hydrogenation of ethylbenzene to reactive ethyl cyclohexane intermediate at the Pt sites, the isomerization of ethyl cyclohexane over the acid sites, and finally dehydrogenation of dimethylcyclohexane to the xylene isomers. It could be reported by Silva et al. that in the case of Pt-containing bifunctional catalysis, the effect of platinum on the thermodynamic equilibrium of xylenes (ATE) can be neglected [49].

The results obtained from the quantitative coke rate deposition (Table 4) show that the rate of coke formation in FeY nanocatalysts is much lower than the amount deposited in the parent HY nanocatalyst. Given the important role of the Lewis acid sites in coke deposition [42,48], it can be concluded that the reduction of these sites by the addition of iron leads to a decrease in the amount of coke formed in the nanocatalyst and ultimately increases its stability.

A comparison of the results related to the conversion EB (%) and the distribution of products (wt.%) in the EB transformation process using synthesized nanocatalysts and the results presented in other studies is given in Table 5. Although it is difficult to compare the results due to different laboratory conditions directly, it can be observed that the conversion and isomerization of EB using P/1.0FY catalyst is higher than the other presented catalysts. From the test results, PtA-1.0FY nanocatalyst indicated the highest EB conversion and EB isomerization toward other nanocatalysts during 15h of time on stream (TOS), which is due to the suitable balance between metal site and acid function of nanocatalyst.

Table 3 Distribution (wt.%) of the reaction products at EB conversion of 35%.

Catalysts	Distribution (wt.%)					
	Isom[a]	Disp[b]	Dealk[c]	Crack[d]	Hydrog[e]	Transalk[f]
H-Y	0.1	48.3	31.7	2.6	0.1	17.2
0.2FY	0.9	43.5	33.2	1.1	2.1	19.2
0.5FY	1.2	41.8	33.6	1.8	2.5	19.1
1.0FY	2.1	40.9	34.4	1.8	2.6	18.2
P/0.2FY	58.5	17.5	4.8	8.6	8.8	1.8
P/0.5FY	69.3	9.8	3.4	4.6	12	0.9
P/1.0FY	77.2	3.3	1.4	3.1	14.8	0.2

[a] somerization
[b] Disproportionation
[c] Dealkylation
[d] Cracking
[e] Hydrogenation
[f] Transalkylation

Table 4 Coke quantity and deposition rate for EB transformation over different nanocatalysts samples.

Nanocatalyst	Coke deposited (wt.%)	Coke deposition rate (wt.%/h)
HY	7.51	0.50
PtA/0.2FY	4.22	0.28
PtA/0.5FY	3.98	0.26
PtA/1.0FY	3.38	0.22

Note: the amount of coke deposited was calculated after TOS of 15h by the weight loss of nanocatalysts upon the Thermogravimetric analysis. The coke deposition rate was determined in order: Total coke quantity (wt.%)/15h

Table 5 The EB conversion and products distributions over different nanocatalysts samples.

Catalyst	EB conversion (%)	Isomerization (%)	Reference
PtA/HMOR120	35	60.1	[52]
2PtA-EUO(75/25)	60	47	[13]
B_2	77.9	43.8	[50]
M_2	73.2	41.4	[50]
2PtA/28NaHMOR10(95/5)	35	71.3	[54]
Pt/Al_2O_3-ZSM-5	35	2	[55]
Pt/Al_2O_3-Ferrierite	35	18	[55]
Pt/Al_2O_3-ZSM-22	35	40	[55]
Pt/Al_2O_3-EU-1	35	17	[55]
Pt/Al_2O_3-Mordenite	35	68	[55]
P/1.0FY	61	77.2	Present study

Conclusions

FeY nanocatalysts containing Pt (PtA-FeY) were synthesized through physical mixing of FeY nanocatalysts and Pt/Alumina, and they were characterized for EB transformation reactions.

The morphology of synthesized Y powders demonstrated hexagonal crystallites with an average crystal size of 30 nm. The introduction of Fe ions into zeolite Y slightly decreased the surface area.

The very slight decrease in the surface area of synthesized Fe-containing nanocatalysts indicated that the major part of iron is in the catalyst structure and a small amount of it is on the surface of the samples.

The balance between the acid and metal sites of the prepared nanocatalysts illustrated the great importance in the EB isomerization process.

Characterization data have demonstrated that Fe ion exchange to the nanozeolite framework reduces the Lewis acid sites while forming new Brönsted acid sites.

The introduction of Fe ions into zeolite Y slightly decreased the surface area from 786.23 m^2/g for the nanozeolite H-Y to 763.89 m2/g for 1.0 FY.

Exchanging the acid sites of Y nanocatalysts with iron caused an increase in the selectivity to disproportionation and dealkylation and cracking while significantly increasing the nanocatalyst stability.

Moreover, the introduction of PtA into Fe-Y nanocatalysts leads to an increase in the selectivity to isomerization and hydrogenation. At the same time, diminishment has been occurred in the selectivity to other unwanted reactions. The decrease in weak acidity reduced coke formation and increased the stability of the optimized nanocatalyst. Ultimately, P/1. 0FY catalyst indicated to be more efficient than other prepared nanocatalysts with 61% conversion and 77.2% isomerization of EB.

Nomenclatures and Abbreviations

C: Cylinder
NV: Needle Valve
PI: Pressure indicator
GC: Gas Chromatography
GCS: Gas Collector System
MFC: Mass Flow Controller
MFM: Mass Flow Meter
NRV: Non-Return Valve
FT: Feed Tank
PRV: Pressure Regulator Valve
R: Reactor
TIC: Temperature Indicator & Collector
SP: Syringe Pump
3WV: 3-Way Valve
PX: Para xylene
MX: Meta xylene
OX: Ortho xylene
EB: Ethyl benzene
SEM: Scanning Electron Microscopy
BET: Brunauer–Emmett–Teller
XRD: X-ray diffraction
FTIR: Fourier-transform infrared spectroscopy
ICP: Inductively coupled plasma
TPD: Temperature-programmed desorption
NMR: Nuclear Magnetic Resonance
TG: Thermogravimetric Analysis
FAU: Faujasite
DMCHE: Dimethylcyclohexane
ECHE: Ethylcyclohexane
DMEB: Dimethylethylbenzene

Acknowledgement

The authors gratefully acknowledge Iran Polymer and Petrochemical Institute (IPPI) (Technological project with grant No: 51793101).

Interest Statement

The authors declare no conflict of interest.

Contributions Statement

Nakisa Yaghobi conceived and supervised the research. Milad Rasouli and Ehsan Shekarian designed the experiments. Milad Rasouli and Ehsan Shekarian performed most of the experiments and data analysis. Milad Rasouli wrote the paper with support from Nakisa Yaghobi. All authors discussed the results and commented on the manuscript.

References

1. Al-Khattaf S, Rabiu S, Tukur N, Alnaizy R (2008) Kinetics of toluene methylation over USY-zeolite catalyst in a riser simulator, Chemical Engineering Journal, 139: 622-630.
2. Gonçalves JC, Rodrigues AE (2013) Thermodynamic equilibrium of xylene isomerization in the liquid phase, Journal of Chemical and Engineering Data, 58: 1425-1428.
3. Min HK, Cha SH, Hong SB (2012) Mechanistic insights into the zeolite-catalyzed isomerization and disproportionation of m-xylene, ACS Catalysis, 2: 971-981.
4. Shah J, Jan MR (2015) Effect of polyethylene terephthalate on the catalytic pyrolysis of polystyrene: Investigation of the liquid products, Journal of the Taiwan Institute of Chemical Engineers, 51: 96-102.
5. Tukur NM, Al-Khattaf S (2011) Comparison studies of xylene isomerization and disproportionation reactions between SSZ-33, TNU-9, mordenite and ZSM-5 zeolite catalysts, Chemical Engineering Journal, 166: 348-357.
6. Rasouli M, Yaghobi N, Allahgholipour F, Atashi H (2014) Para-xylene adsorption separation process using nano-zeolite Ba-X, Chemical Engineering Research and Design, 92: 1192-1199.
7. Rasouli M, Yaghobi N, Chitsazan S, Sayyar MH (2012) Influence of monovalent cations ion-exchange on zeolite ZSM-5 in separation of para-xylene from xylene mixture, Microporous and Mesoporous Materials, 150: 47-54.
8. Rasouli M, Yaghobi N, Gilani SZM, Atashi H, Rasouli M (2015) Influence of monovalent alkaline metal cations on binder-free nano-zeolite X in para-xylene separation, Chinese Journal of Chemical Engineering, 23: 64-70.
9. Aboul-Gheit AK, Aboul-Fotouh SM (2012) Insight in cyclohexene hydroconversion process using catalysts containing 0.35% Pt on amorphous and zeolite supports, Journal of the Taiwan Institute of Chemical Engineering, 43: 711-717.
10. Daramola M, Burger A, Giroir-Fendler A (2011) Modelling and sensitivity analysis of a nanocomposite MFI-alumina based extractor-type zeolite catalytic membrane reactor for m-Xylene isomerization over Pt-HZSM-5 catalyst, Chemical Engineering Journal, 171: 618-627.
11. Guillon E, Lacombe S, Sozinho T (2009) How to improve the selectivity of zeolitic catalysts in C8 aromatic cut isomerization, Oil and Gas Science and Technology-Revue de l'IFP, 64: 731-744.
12. Tarach KA, Gołąbek K, Choi M, Góra-Marek K (2017) Quantitative infrared spectroscopic studies and 2D COS analysis of xylenes isomerization over hierarchical zeolites, Catalysis Today, 283: 158-171.
13. Moreau F, Moreau P, Gnep NS (2006) Ethylbenzene isomerization over bifunctional platinum alumina–EUO catalysts: Location of the active sites, Microporous and Mesoporous Materials, 90: 327-338.
14. Iskandar F, Afifah Zen N, Rona Mayangsari T, Hasdi Aimon A, Astra Pramana A (2019) Development of faujasite-type zeolite and iron oxide as mixed catalyst for aquathermolysis reaction of heavy oil, Materials Research Express. 6.
15. Shekarian E, Jafari Nasr MR, Mohammadi T, Bakhtiari O, Javanbakht M (2019) Preparation of 4A zeolite coated polypropylene membrane for lithium-ion batteries separator, Journal of Applied Polymer Science, 136: 47841.
16. Jia X, Han L, Ma Y, Che S (2018) Additive-free synthesis of mesoporous FAU-type zeolite with intergrown structure, Science China Materials, 61: 1095-1100.
17. Wang L, Xiao FS (2018) A significant enhancement of catalytic performance by adjusting catalyst wettability,

Science China Materials, 61: 1137-1142.
18. Farahani SH, Alavi SM, Falamaki C (2017) Improved performance of HZSM-5 for the ethylbenzene/xylene isomerization reaction under industrial operating conditions, RSC Advances, 7: 34012-34022.
19. Farshadi M, Falamaki C (2018) Ethylbenzene disproportionation and p-xylene selectivity enhancement in xylene isomerization using high crystallinity desilicated H-ZSM-5, Chinese Journal of Chemical Engineering, 26: 116-126.
20. Shi Q, Gonçalves JC, Ferreira AF, Plaza MG, Rodrigues AE (2018) Xylene isomerization side reactions over Beta zeolite: Disproportionation and transalkylation of C8 aromatics and toluene, Applied Catalysis A: General, 562: 198-205.
21. Shi Q, Gonçalves JC, Ferreira AF, Plaza MG, Rodrigues AE (2018) Xylene Isomerization over Beta Zeolites in Liquid Phase, Industrial & Engineering Chemistry Research, 57: 5568-5579.
22. Yanna L, Jingyang X, Lijun J, Yunming F, Haoquan H (2009) Synthesis and modification of zeolite NaA adsorbents for separation of hydrogen and methane, Asia-Pacific Journal of Chemical Engineering, 4: 666-671.
23. Moreau F, Bernard S, Gnep NS, Lacombe S, Merlen E, Guisnet M (2001) Ethylbenzene isomerization on bifunctional platinum alumina–mordenite catalysts 1. influence of the mordenite Si/Al Ratio, Journal of Catalysis, 202: 402-412.
24. Geetha Bhavani A, Pandurangan A (2007) Hydroisomerization of ethylbenzene over bimetallic bifunctional zeolite catalysts, Journal of Molecular Catalysis A: Chemical, 267: 209–217.
25. Tsai TC, Wang I, Huang CK, Liu SD (2007) Study on ethylbenzene and xylene conversion over modified ZSM-5, Applied Catalysis A: General, 321: 125–134.
26. Rasouli M, Yaghobi N, Chitsazan S, Sayyar MH (2012) Effect of nanocrystalline zeolite Na-Y on meta-xylene separation, Microporous and Mesoporous Materials, 152: 141-147.
27. Ruiping W, Maiping G, Jun W (2009) Preparation, characterization and catalytic behavior of 12-molybdophosphoric acid encapsulated in the supercage of Cs+-exchanged Y zeolite, Chinese Journal of Chemical Engineering, 17: 58-63.
28. Liu SQ, Cheng S, Feng LR, Wang XM, Chen ZG (2010) Effect of alkali cations on heterogeneous photo-Fenton process mediated by Prussian blue colloids, Journal of hazardous materials, 182: 665-671.
29. Haghighi Asl M, Sargolzaei J, Moosavi F (2015) Identification of the coke deposited on 13X industrial zeolite molecular sieves during mercaptan removal process, Asia-Pacifif Journal of Chemical Engineering 11: 164-178.
30. Sanaeepur H, Kargari A, Nasernejad B, Amooghin AE, Omidkhah M (2016) A novel $Co2^{+}$ exchanged zeolite Y/ cellulose acetate mixed matrix membrane for CO_2/N_2 separation, Journal of the Taiwan Institute of Chemical Engineers, 60: 403-413.
31. [31] Jian Z, Zhicheng L, Liyuan L (2013) Hierarchical mesoporous ZSM-5 zeolite with increased external surface acid sites and high catalytic performance in o-xylene isomerization, Chinese Journal of Catalysis, 34: 1429-1433.
32. Toch K, Thybaut J, Vandegehuchte B (2012) A Single-Event MicroKinetic model for ethylbenzene dealkylation/xylene isomerization on Pt/H-ZSM-5 zeolite catalyst, Applied Catalysis A: General., 425: 130-144.
33. Haji S, Khalaf M, Shukrallah M, Abdullah J, Ahmed S (2015) A kinetic comparative study of azo dye decolorization by catalytic wet peroxide oxidation using Fe–Y zeolite/H_2O_2 and photooxidation using UV/H_2O_2, Reaction Kinetics, Mechanisms and Catalysis, 114: 795-815.
34. Rostamizadeh M, Yaripour F (2016) Bifunctional and bimetallic Fe/ZSM-5 nanocatalysts for methanol to olefin reaction, Fuel., 181: 537-546.
35. Kondru AK, Kumar P, Chand S (2009) Catalytic wet peroxide oxidation of azo dye (Congo red) using modified Y zeolite as catalyst, Journal of Hazardous Materials, 166: 342-347.
36. Aravindhan R, Fathima NN, Rao JR, Nair BU (2006) Wet oxidation of acid brown dye by hydrogen peroxide using heterogeneous catalyst Mn-salen-Y zeolite: a potential catalyst, Journal Hazard Mater, 138: 152-159.
37. Heuchel M, Dörr C, Boldushevskii R (2018) The influence of porosity and active sites of zeolites Y and beta on the co-cracking of n-decane and 2-ethylphenol, Applied Catalysis A: General, 553: 91-106.
38. Soltanali S, Hajjar Z, Bahadoran F (2019) The possibility of phase change in amorphous silica-alumina synthesis to FAU zeolite using carbon nano structures, Materials Research Express, 6.
39. Wang JQ, Huang YX, Pan Y, Mi JX (2016) New hydrothermal route for the synthesis of high purity nanoparticles of zeolite Y from kaolin and quartz, Microporous and Mesoporous Materials, 232: 77-85.
40. Pedrosa AMG, Souza MJ, Melo DM, Araujo AS (2006) Cobalt and nickel supported on HY zeolite: Synthesis, characterization and catalytic properties, Materials Research Bulletin. 41: 1105-1111.
41. Cui Q, Wang S, Wei Q (2019) Synthesis and characterization of Zr incorporated small crystal size Y zeolite supported NiW catalysts for hydrocracking of vacuum gas oil, Fuel., 237: 597-605.
42. Qu Z, Roduner E (2009) In situ ESR study of gold supported on NaY zeolite, Asia-Pacific Journal of Chemical Engineering, 4: 602-606.
43. Hosseinpour N, Khodadadi AA, Mortazavi Y, Bazyari A (2009) Nano-ceria–zirconia promoter effects on enhanced coke combustion and oxidation of CO formed in regeneration of silica–alumina coked during cracking of triisopropylbenzene, Applied Catalysis A: General, 353: 271-281.
44. Chu Y, Yi X, Li C, Sun X, Zheng A (2018) Brønsted/ Lewis acid sites synergistically promote the initial C–C bond formation in the MTO reaction, Chemical science, 9: 6470-6479.
45. Lee S, Choi M (2019) Unveiling coke formation

mechanism in MFI zeolites during methanol-to-hydrocarbons conversion, Journal of Catalysis 375, 183-192.
46. Dai J, Zhang H (2019) Recent advances in selective CC bond coupling for ethanol upgrading over balanced Lewis acid-base catalysts, Science China Materials, 1-13.
47. Du H, Olson DH (2002) Surface acidic properties of a HMCM-22 zeolite: Collidine poisoning and hydrocarbon adsorption studies, The Journal of Physical Chemistry B, 106: 395-400.
48. McCaulay DA, Lien AP (1953) Disproportionation of alkylbenzenes.II. Mechanism of alkyl-group transfer, Journal of American Chemical Society, 75, 10: 2411–2413.
49. Silva J, Ribeiro M, Ribeiro FR, Benazzi F, Guisnet M (1995) Transformation of an ethylbenzene-o-xylene mixture on HMOR and Pt-HMOR catalysts. Comparison with ZSM-5 catalysts, Applied Catalysis A: General, 125: 15-27.
50. Bhavani AG, Pandurangan A (2007) Hydroisomerization of ethylbenzene over bimetallic bifunctional zeolite catalysts, Journal of Molecular Catalysis A: Chemical, 267: 209-217.
51. Rasouli M, Yaghobi N (2018) Synthesis and characterization of platinum impregnated Zn-Zsm5 nanocatalysts for xylene isomerization reactions, Catalysis Letters, 148: 2325-2336.
52. Gnep N, de Armando MM, Guisnet M (1983) O-Xylene transformation on acid catalysts: influence of hydrogen activated on metallic sites, studies in surface science and catalysis, Elsevier, 17: 309-318.
53. Moreau F, Bernard S, Gnep N (2001) Ethylbenzene isomerization on bifunctional platinum alumina–mordenite catalysts: 1. Influence of the mordenite Si/Al ratio, Journal of Catalysis, 202: 402-412.
54. Moreau F, Gnep N, Lacombe S, Merlen E, Guisnet M (2002) Ethylbenzene transformation on bifunctional Pt/Al_2O_3-NaHMOR catalysts: Influence of Na exchange on their activity and selectivity in ethylbenzene isomerization, Applied Catalysis A: General, 230: 253-262.
55. Moreau P, Gnep N, Magnoux P (2008) Influence of zeolite structure on ethylbenzene transformation, Studies in Surface Science and Catalysis, Elsevier, 174: 1179-1182.